

The Photonic Band theory and the negative refraction experiment of metallic helix metamaterials

Chao Wu,¹ Hongqiang Li,^{1,*} Zeyong Wei,¹ Xiaotong Yu,¹ and C.T. Chan²

¹Physics Department, Tongji University, Shanghai 200092, China

²Department of Physics, Hong Kong University of Science and Technology, Clear Water Bay, Kowloon, Hong Kong, China

We develop a theory to compute and interpret the photonic band structure of a periodic array of metallic helices for the first time. Interesting features of band structure include the ingenious longitudinal and circularly polarized eigenmodes, the wide polarization gap [Science **325**, 1513 (2009)], and the helical symmetry guarantees the existence of negative group velocity bands at both sides of the polarization gap and band crossings pinned at the zone boundary with fixed frequencies. A direct proof of negative refraction via a chiral route [Science **306**, 1353 (2004)] is achieved for the first time by measuring Goos-hanchen shift through a slab of three dimensional bona fide helix metamaterial.

PACS numbers: 78.67.Pt, 42.70.Qs, 42.25.Ja

With a pitch angle accounting for mirror asymmetry, a helix is a prototype element of chiral media. As a pioneer study, the electromagnetic(EM) activity from randomly dispersed metallic helices was observed in 1914 [1]. After the prediction on negative refraction via chiral route [2], chiral metamaterials have been arousing more and more attentions recently on negative refraction index [3–6], strong optical activity [7–9] and circular dichroism [10–13] as well. In the most of previous studies, chiral metamaterials are typically realized as one or two layers of discrete chiral resonators and the negative refractive index is deduced indirectly from retrieval procedures [3–6] assuming the applicability of effective medium theory [14–18]. Recently, the Gold helix metamaterial with a few pitches along the helical axis are successfully fabricated in THz regime with a wide polarization gap measured experimentally [19], which also raised a question whether the effective medium theory is enough for the description of chiral metamaterials. To the best of our knowledge, most previous studies adopt effective medium description and well-defined EM parameters for theoretical analysis, and empirically interpret the exotic properties in a numerical stage. While there is no any “first-principle” investigation starting from the real structure of chiral metamaterial. Also it is worth noting that in all previous studies, negative refraction indices, retrieved from the transmission and reflection spectra under normal incidence, do not give any direct proof for negative refraction. The negative refraction via chiral route hasn’t really achieved before.

In this paper, we theoretically and experimentally investigate the properties of a three-dimensional metamaterial made with a square array of metallic helices. We develop a photonic band theory for helix metamaterial by combining Multiple Scattering Theory (MST) [20, 21] with Sensiper’s solution for a single helix [22]. The theory enables us to identify the longitudinal and circularly polarized eigenmodes, the formation of the wide polarization gap, negative group velocity bands at both sides of the gap and related fine features. We also demonstrate a proof of principle

experiment by measuring negative Goos-hanchen shift to directly verify the negative refraction from helix metamaterial for the first time.

Figure 1 shows a photograph of a sample of the three-dimensional metamaterial comprising a square array of right-handed (RH) helices. Oriented along the z axis, the metallic helices form a square array in the xy plane with a lattice constant of $d = 11$ mm. Figure 1(a) shows the schematic picture of a single helix unit, which has a pitch of $p = 4.4$ mm, radius $a = 3.3$ mm, and diameter of metallic wires $\delta = 0.8$ mm. We define a pitch angle ψ by $\cot \psi = 2\pi a/p$. We note that a helix comes back to itself after being translated by a distance of Δz and being rotated simultaneously by a angle of $2\pi\Delta z/p$ (for RH helix) or $-2\pi\Delta z/p$ [for left-handed (LH) helix], and thus physical entities associated with the helix should satisfy the helical symmetry condition

$$U(\rho, \phi, z) = U\left(\rho, \phi \pm \frac{2\pi\Delta z}{p}, z + \Delta z\right) \quad (1)$$

with \pm sign for the RH/LH helix respectively [22, 23]. As the helical system is also periodic along the helical axis, the field components for an RH helix system can be expanded by functions of the form

$$\psi_n(\rho, \phi, z) = e^{ik_z z} F_n(\rho) e^{-in\phi} e^{i\frac{2n\pi}{p} z} \quad (2)$$

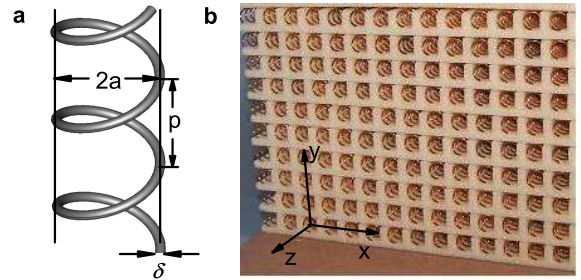


FIG. 1: (a) The schematic picture of a metallic helix unit and (b) photo of a square array of metallic helices.

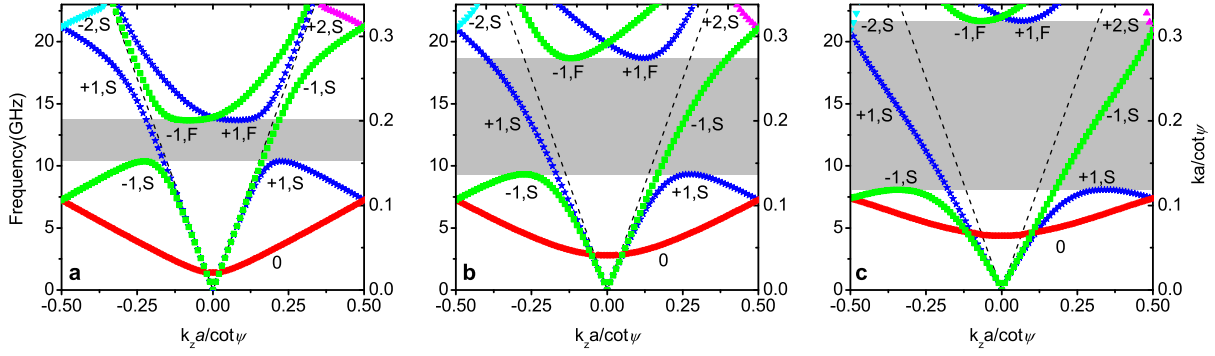


FIG. 2: The photonic band structures of the helix crystal along the helix axis for three lattice constants (a) $d = 20$ mm, (b) $d = 11$ mm, (c) $d = 8$ mm. The pitch $p = 4.4$ mm, the radius $a = 3.3$ mm, and diameter of metallic wires $\delta = 0.8$ mm.

where k_z is the Bloch wavevector along z axis. The angular term should be $e^{in\phi}$ instead if the helix is LH. The radial function $F_n(\rho)$ obeys the Helmholtz differential equation, and can be expressed in terms of modified Bessel functions I_n and K_n . We follow the Sensiper approach [22] to impose the assumption about uniformly distributed surface current flow along the metal wires. Under that assumption, the boundary continuity conditions require that the local electric field on metal wires must be perpendicular to the line of metal wire. Thus we derive an eigenvalue equation of helix array by MST as

$$\sum_n \left[\left(k_z^2 a^2 - k^2 a^2 + \frac{n^2 k^2}{\tau_n^2} \cot^2 \psi \right) y_n I_n(\tau_n a) + k^2 a^2 \cot^2 \psi z_n I'_n(\tau_n a) \right] \frac{R_n}{x_n \tau_n} = 0 \quad (3)$$

where $\tau_n = \left[(k_z + \frac{2\pi n}{p})^2 - k^2 \right]^{\frac{1}{2}}$, $R_n = \frac{\sin(n\pi\delta/p)}{n\pi\delta/p}$, $y_n = K_n(\tau_n a) + (-1)^n \sum_l S_{l-n}(\tau_n) I_l(\tau_n a)$, $z_n = K'_n(\tau_n a) + (-1)^n \sum_l S_{l-n}(\tau_n) I'_l(\tau_n a)$, $x_n = y_n I'_n(\tau_n a) - z_n I_n(\tau_n a)$, and $S_l(\tau) = \sum_{q \neq 0} K_l(\tau R_q) e^{il\phi_q} e^{ik_i \cdot \mathbf{R}_q}$ is a lattice sum

running over the nodes (R_q, ϕ_q) of the square lattice in cylindrical coordinates with \mathbf{k}_i being the transverse component of the wavevector \mathbf{k} in the air, and $I'_n(x)$, $K'_n(x)$ satisfy to $I'_n(x) = dI_n(x)/dx$, $K'_n(x) = dK_n(x)/dx$.

The photonic band structures, computed with the combined technique above stated, afford us an intuitive understanding about optics of helix metamaterials. In the helical structure, there is always a $\pi/2$ or $-\pi/2$ phase difference between the radial and the angular components for both the electric field and magnetic field, implying that the eigenmodes are ingenious left-handed or right handed circularly polarized (LCP or RCP). This can be checked by examining the field solutions written in the Sensiper form[22], or by examining the solution from commercial numerical solver CST. Figures 2(a), 2(b) and 2(c) show the band structure of the helix metamaterials along the helix axis for

three lattice constants $d = 20$ mm, 11 mm and 8 mm respectively. We label the eigenmodes by its dominant term in Eq. (2). For example, the $(-1,S)$ modes (blue stars in Fig. 2) have $n = -1$ term as the dominant term and “S” stands for a “slow mode” below the light line, and we use the subscript “F” for a mode inside the light cone. The lowest frequency branch (red circles), labeled as (0) in Fig. 2, has a strong longitudinal component and this mode picks up a LH character as k_z increases. It goes to a longitudinal mode with a finite frequency at Brillouin zone (BZ) center ($k_z = 0$). Both the electric field and magnetic field are essentially parallel to the helical axis. It is evident from Fig. 2 that the inter-helix coupling pushes the longitudinal mode to higher frequencies. In the limit $d \rightarrow \infty$, it goes to zero frequency. The polarization of an eigenmode is analyzed by the ratios $|\langle E_z \rangle| / |\langle E_x \rangle|$, $|\langle E_z \rangle| / |\langle E_y \rangle|$ and $AR = \langle E_x \rangle k_z / \langle iE_y \rangle |k_z|$, where the spatial average, $\langle \dots \rangle$, is taken inside a unit cell. Figure 3 clearly indicate that the polarization of $n = 0, \pm 1$ eigenmodes are longitudinal and/or LCP, RCP exclusively. Eigenmode analysis and numerical transmission simulation employing a finite thickness slab showed that the $n = -1$ modes with positive group velocity (blue stars in Fig. 2) couple to incident plane wave with opposite handedness as the helix, while the $n = +1$ modes with positive group velocity (green squares in Fig. 2) couple to incident waves of the same handedness as the helix. In general, a mode couples to incident wave of the same (opposite) handedness as the helix if $n \cdot k_z > 0 (< 0)$.

An important feature of the band structure is the existence of a wide polarization gap (shaded in grey in Fig. 2) that only allows incident waves of opposite handedness to pass through. As such, a RH helix array has a right-handed circularly polarized (RCP) gap. The gap grows wider for a higher helix filling ratio (smaller d). Such wide polarization gaps have been experimentally demonstrated for a thin slab of gold helices in IR frequencies [19, 24]. The lower edge of the polarization gap is pinned at the frequency at which the $(+1,S)$ mode attains zero group velocity. The $(+1,S)$ mode is the result of the hybridization between the

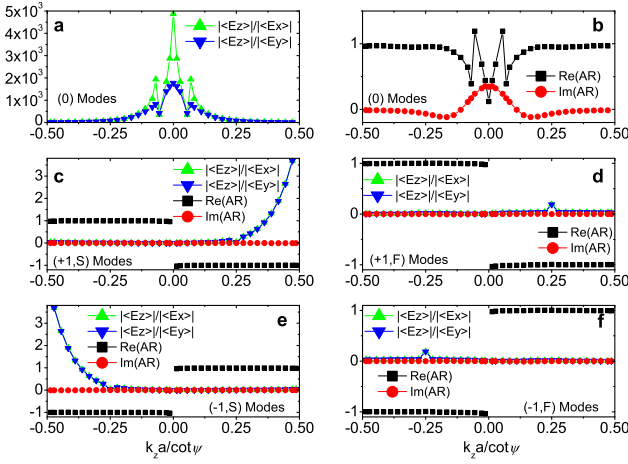


FIG. 3: Eigenmode analysis by calculating the ratios $AR = \langle E_x \rangle k_z / \langle iE_y \rangle |k_z|$, $|\langle E_z \rangle| / |\langle E_x \rangle|$ and $|\langle E_z \rangle| / |\langle E_y \rangle|$. (a) and (b) for $n = 0$ modes; (c) (+1,S) modes; (d) (+1,F) modes; (e) (-1,S) modes; (f) (-1,F) modes.

free photons (riding on the light line) and a mode guided on the helix which is strongly back-scattered by the periodicity. As the (+1,S) mode is guided on the helices, the frequency is only moderately affected by the inter-helix coupling. The upper edge of the polarization gap is pinned at the frequency at which the (+1,F) mode has zero group velocity. The (+1,F) mode is not a guided mode on a single helix. It exists as an eigenmode only in the periodic array and is sensitive to the volume available between the helices and the mode is squeezed to higher frequencies at a higher helix filling ratio, leading to a much bigger polarization gap for smaller values of the lattice constant (d). In other words, the lower edge of the gap is primarily determined by the helix parameters (a and p) along the helical axis, while the upper edge is primarily determined by the structural parameter perpendicular to the helical axis (lattice constant d).

Another interesting feature of the band structure is the emergence of the negative group velocity bands at both sides of the polarization gap, which is different from the previous notions that the negative refraction only happens above the resonant gap. Both the high frequency (+1,F) and the lower frequency (+1,S) branch exhibit negative group velocities. The (+1,S) branch has negative group velocity after reaching a maximum frequency that pins the lower edge of the polarization gap. Concomitant with the negative refraction bands in slow mode, one can see that there are no band gap but band crossings at the BZ boundary ($k = \pi/p$) and the degenerate modes are pinned at fixed frequencies that are nearly independent of lattice constant p . We note that according to Eq. 2 Bloch modes that differ by $\Delta k = 2\pi/p$ will be orthogonal because of orthogonality of the angular phase factor. And the (0) branch degenerates with the (+1,S) branch at zone center, giving rise to a negative group velocity band below the polarization

gap. This is essentially a consequence of backward waves guided on metallic helix satisfying to helical symmetry. As a proof, a comparative study shows that the negative dispersion band disappears as well as other unique features, such as the longitudinal mode, band crossing etc. when the helix metamaterial is cut in a “discrete” form by inserting an 0.4mm air gap at each period(p).

We performed negative refraction measurements inside an anechoic chamber through a slab of the helix metamaterial with the aforementioned geometric parameters [the band structure is shown in Fig. 2(b)]. Helix metamaterial samples are fabricated by periodically embedding the clockwise metallic helices in a polyurethane foam slab. The polyurethane foam slab is lossless with $\epsilon \approx 1$. The sample slab contains 15×11 metallic helices, each having 140 periods along helical axis (z axis).

Computed equi-frequency surface (EFS) for the (+1,S) branch [see Fig. 4(b)] and (+1,F) branch (not shown) demonstrate that negative refraction can be achieved at both sides of the polarization gap. Here we try to realize the negative refraction at the lower edge of the gap, which is not found or predicted in other systems before. As the $(\pm 1, S)$ modes lie below the light line, we can excite the $(\pm 1, S)$ modes by prism coupling techniques to penetrate a Gaussian beam into the sample slab [see Fig. 4(a)], and estimate the refractive angle quantitatively by measuring the Goos-Hanchen shift of the beam. Figure 4(a) illustrates the schematic configuration of our experimental setup. Two isosceles right-angled triangular alumina prisms ($\epsilon_r = 8.9$) are placed so that they touch the sample slab at both sides and a Gaussian beam is normally incident in xz plane to the air-prism interface from a linearly polarized horn emitter (operating at 8.2-12.4 GHz with a gain factor of 24.6 dB), ensuring an incident angle of 45° from alumina to metamaterial. The local field intensity is measured by the LCP/RCP horn receiver as a function of the horizontal position in a precision of 1 mm per step. The Goos-Hanchen shift of the outgoing beam is quantified by measuring the peak position at the interface of prism. The coordinate origin in the horizontal position is aligned to the position of the horn emitter, marked by the dashed vertical line in Fig. 4(a). The negative refraction is measured from 9.18 GHz to 9.48 GHz with a refraction angle from -17.44° to -50.11° , which is in good agreement with the computed equi-frequency surface (EFS) shown in Fig. 4(b). The solid line in Fig. 4(d) presents the spatial profile of local field intensity measured at 9.41 GHz. A peak value is measured at the horizontal position of -24 cm, corresponding to a refraction angle of -46.45° , roughly equal to -45.82° estimated by EFS analysis. Thus negative refraction below the polarization gap is verified experimentally. Negative refraction is also qualitatively verified by finite-difference-in-time-domain (FDTD) simulations shown in Fig. 4(c). We note from Fig. 4(b) that in the frequency range of our interest, the dispersion is not only negative along k_z , but it is also negative along k_x due to

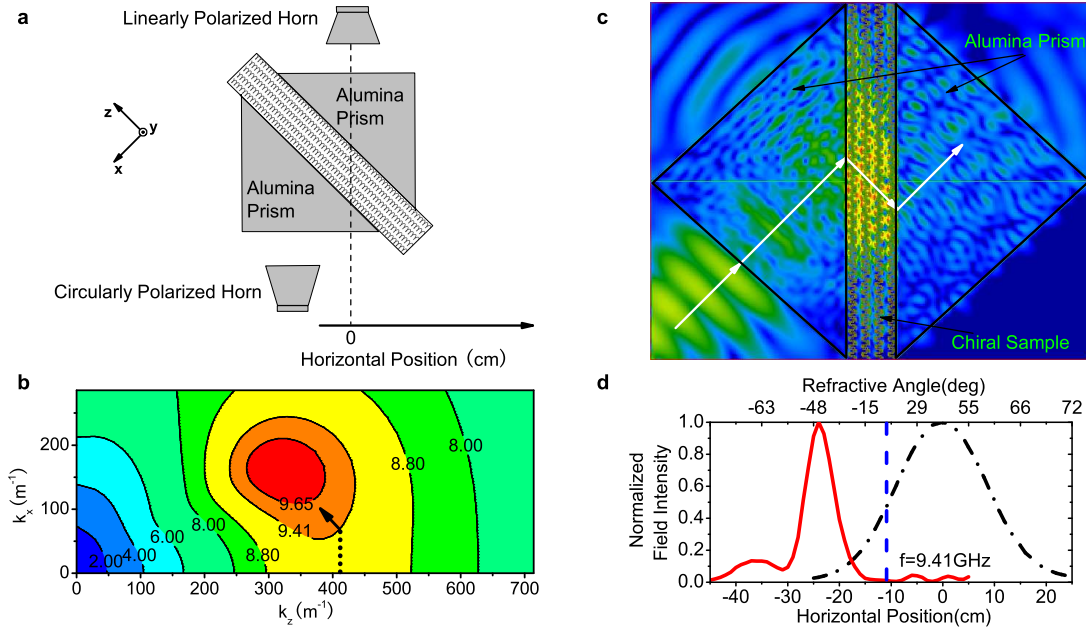


FIG. 4: (a) Schematic of the experimental setup for negative refraction. (b) Computed equi-frequency surface (EFS) for the (+1,S) branch. The arrow refers to the direction of the refracted waves at 9.41 GHz under an incident angle at 45° . (c) FDTD simulations of negative refraction. In calculation, an RCP Gaussian beam with a frequency $f = 9.41$ GHz is normally impinging on the left prism. The chiral sample has 4×5 helices in the xy plane and 45 periods along the z axis. The direction of energy flow is indicated by the arrow. (d) Measured electric field intensity as a function of the horizontal position of the circularly polarized horn receiver, with (red) or without (black) the chiral sample and alumina prisms at 9.41 GHz. The two curves are normalized such that the magnitude of both peaks is unity. The blue dashed line at horizontal position of -11 cm refers to Goos-Hanchen shift with respect to 0° refracted angle.

Bragg scattering.

In summary, we witness the mathematical beauty of wave propagation in metallic helix metamaterial by analytical resolved photonic band structure. There are negative bands both above and below the polarization gap. Negative refraction on the low frequency branch is demonstrated directly for the first time by a Goos-Hanchen shift experiment. We note that the optics of helix metamaterial is governed by the collective selection on the guided modes on helices satisfying to helical symmetry and (evanescent) Bragg scatterings within helix lattice and in passing there is no easy way to describe the phenomena using effective medium parameters. This work was supported by NSFC (No. 10974144, 60674778), HK RGC grant 600308, the National 863 Program of China (No.2006AA03Z407), NCET (07-0621), STCSM and SHEDF (No. 06SG24). We thank for M. Wegener and J. Gansel for helpful discussions.

* Electronic address: hqlee@tongji.edu.cn

- [1] I. V. Lindell, A. H. Sihvola, and J. Kurkijarvi, IEEE Trans Ant. & Prop. **34**, 24 (1992).
- [2] J. B. Pendry, Science **306**, 1353 (2004).
- [3] E. Plum et al., Phys. Rev. B **79**, 035407 (2009).
- [4] S. Zhang et al., Phys. Rev. Lett. **102**, 023901 (2009).

- [5] J. Zhou et al., Phys. Rev. B **79**, 121104(R) (2009).
- [6] M. C. K. Wiltshire, J. B. Pendry, and J. V. Hajnal, J. Phys.: Condens. Matter **21**, 292201 (2009).
- [7] E. Plum et al., Appl. Phys. Lett. **90**, 223113(2007).
- [8] H. Liu et al., Phys. Rev. B **76**, 073101 (2007).
- [9] T. Q. Li et al., Appl. Phys. Lett. **92**, 131111 (2008).
- [10] S. L. Prosvirnin, and N. I. Zheludev, Phys. Rev. E **71**, 037603 (2005).
- [11] A. V. Krasavin et al., Appl. Phys. Lett. **86**, 201105 (2005).
- [12] V. A. Fedotov et al., Phys. Rev. Lett. **97**, 167401 (2006).
- [13] E. Plum et al., Phys. Rev. Lett. **102**, 113902 (2009).
- [14] N. Engheta, D. L. Jaggard, and M. W. Kowarz, IEEE Trans Ant. & Prop. **40**, 367 (1992).
- [15] S. Tretyakov et al., J. Electron Waves and Appl. **17**, 695 (2003).
- [16] T. G. Mackay, and A. Lakhtakia, Phys. Rev. E **69**, 026602 (2004).
- [17] C. Monzon, and D. W. Forester, Phys. Rev. Lett. **95**, 123904 (2005).
- [18] Q. Cheng, and T. J. Cui, Phys. Rev. B **73**, 113104 (2006).
- [19] J. K. Gansel et al., Science **325**, 1513 (2009).
- [20] S. K. Chin, N. A. Nicorovici, and R. C. McPhedran, Phys. Rev. E **49**, 4590 (1994).
- [21] N. A. Nicorovici, R. C. McPhedran, and L. C. Botten, Phys. Rev. E **52**, 1135 (1995).
- [22] S. Sensiper, Proc. IRE **43**, 149 (1955).
- [23] J. R. Pierce, Proc. IRE **35**, 111 (1947).
- [24] J. K. Gansel et al., Opt. Exp. **18**, 1059 (2010).